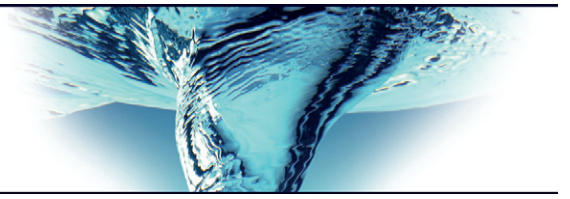
CrossMark

J. Fluid Mech. (2018), *vol.* 848, R3, doi:10.1017/jfm.2018.435



JFM RAPIDS
journals.cambridge.org/rapids

Singular jets during the collapse of drop-impact craters

S. T. Thoroddsen[1,†], K. Takehara[2], H. D. Nguyen[2,3] and T. G. Etoh[2]

[1]Division of Physical Sciences and Engineering, King Abdullah University of Science and Technology (KAUST), Thuwal 23955-6900, Saudi Arabia

[2]Department of Civil and Environmental Engineering, Kindai University, Higashi-Osaka 577-8502, Japan

[3]Hanoi University of Science and Technology, No. 1 Dai Co Viet Street, Hanoi, Vietnam

(Received 28 March 2018; revised 10 May 2018; accepted 12 May 2018; first published online 13 June 2018)

When a drop impacts on a deep pool at moderate velocity it forms a hemispheric crater which subsequently rebounds to the original free-surface level, often forming Worthington jets, which rise vertically out of the crater centre. Under certain impact conditions the crater collapse forms a dimple at its bottom, which pinches off a bubble and is also known to be associated with the formation of a very fast thin jet. Herein we use two ultra-high-speed video cameras to observe simultaneously the dimple collapse and the speed of the resulting jet. The fastest fine jets are observed at speeds of approximately 50 m s^{-1} and emerge when the dimple forms a cylinder which retracts without pinching off a bubble. We also identify what appears to be micro-bubbles at the bottom of this cylinder, which we propose are caused by local cavitation from extensional stress in the flow entering the jet. The radial collapse of the dimple does not follow capillary-inertial power laws nor is its bottom driven by a curvature singularity, as has been proposed in some earlier studies. The fastest jets are produced by pure inertial focusing and emerge at finite dimple size, bypassing the pinch-off singularity. These jets emerge from the liquid contained originally in the drop. Finally, we measure directly the compression of the central bubble following the pinch-off and the subsequent large volume oscillation, which occurs at frequencies slightly above the audible range at approximately 23 kHz.

Key words: bubble dynamics, drops and bubbles, hydrodynamic noise

1. Introduction

1.1. *Crater collapse and singular jets*

Drops impacting on a liquid pool eject a splashing crown, but also form a hemispheric crater. The subsequent rebound of this crater (figure 1) tends to focus the energy into

†Email address for correspondence: sigurdur.thoroddsen@kaust.edu.sa

© Cambridge University Press 2018

https://doi.org/10.1017/jfm.2018.435 Published online by Cambridge University Press

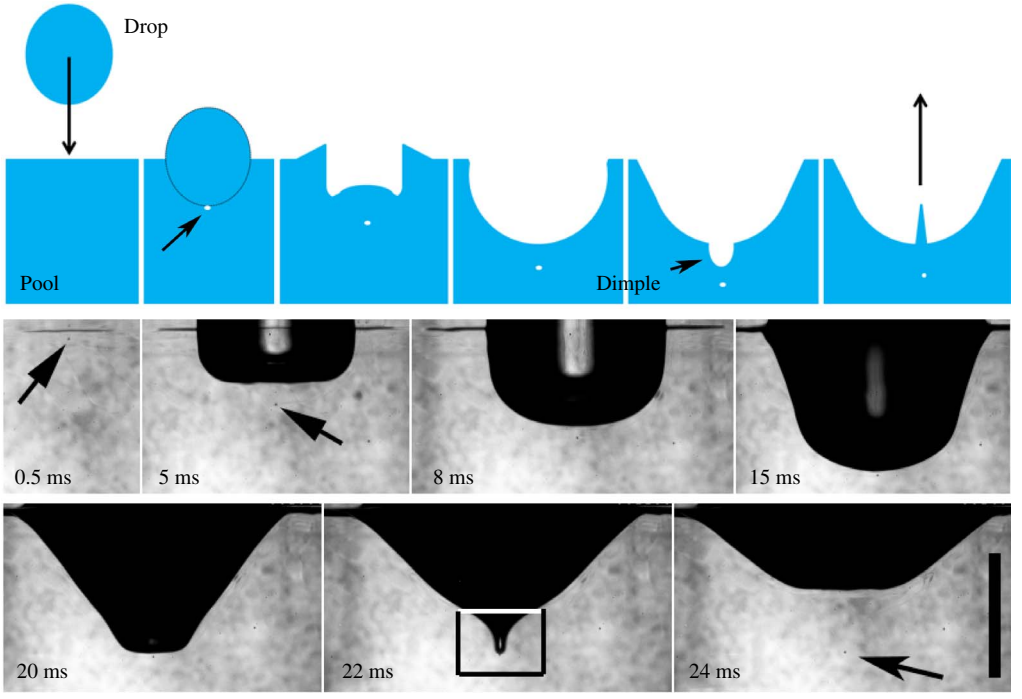


FIGURE 1. Sketch and video frames showing the typical impact crater collapse and jetting. The air crater appears dark under the free surface. Herein we focus the imaging on the dimple, shown inside the rectangle. The arrows indicate the tiny bubble entrapped under the drop as it first hits the free surface. The scale bar is 5 mm.

a Worthington jet which rises from its centre. For low impact velocities the bottom of the crater can form a dimple which pinches off to entrap a small bubble into the pool. This phenomenon was studied by Pumphrey & Elmore (1990) in relation to the underwater sound produced by rain (Prosperetti & Oguz 1993). Oguz & Prosperetti (1990) simulated this phenomenon numerically and suggested bounds in parameter space where this entrapment occurs. The formation of the bottom dimple is connected to capillary waves travelling downwards from the pool surface and focusing at the bottom apex. Similar dynamics occurs for coalescing bubbles (Zhang *et al.* 2015). However, the details are strongly dependent on small changes in the impact conditions, with a limited range where very fine high-speed jets are produced. Rein (1996) used a high-speed film camera to study this connection, but only at 500 fps. Liow (2001) used 3000 fps to characterize the surface shape for the fastest jets, which he attributed to the retraction of a capillary wave without bubble entrapment. Morton, Rudman & Liow (2000) further characterized the capillary waves and the produced vorticity using numerical simulations. More recently Deng, Anilkumar & Wang (2007) studied how liquid viscosity and surface tension affect the dimple shapes, showing how the size of the entrapped bubble scales with capillary number. They show that higher viscosity shifts the entrapment regime to a larger Weber number *We*. Ray, Biswas & Sharma (2015) performed comprehensive simulations of drop-impact crater evolution, reproducing many of the observed dimple shapes, while showing jetting speeds less than five times the drop-impact velocity. However, their 100 μm grid^{-1} resolution would not capture the finest jets observed herein.

https://doi.org/10.1017/jfm.2018.435 Published online by Cambridge University Press

The most comprehensive experimental study of these jets to date is that of Michon, Josserand & Séon (2017), who used 8000 fps. They characterize the fast singular jets as 'barely reproducible', but observe jet velocities up to 14 times the drop-impact velocity.

Zeff *et al.* (2000) looked at a related problem of crater collapse in a vertically oscillated container, in the context of super-critical Faraday waves. They proposed a self-similar capillary-inertial collapse, where the surface curvature diverges, thereby driving the fast-moving fine jet. On the other hand, they used large-viscosity liquid and their observed jet velocities were larger than the corresponding capillary-viscous velocity σ/μ_ℓ, which does not contain a length scale and should therefore give an upper bound for capillary-driven jets (Ganan-Calvo 2017). It is therefore unclear what role surface tension and viscosity play, as discussed in Thoroddsen, Etoh & Takehara (2007*b*), who showed that the focusing of capillary waves on a free-falling drop can generate a fine jet. Das & Hopfinger (2008) have investigated the collapse of parametrically forced waves in more detail.

1.2. *Jets from bursting bubbles at a pool surface*

Closely related jets are generated by the bursting of bubbles sitting under a free liquid surface. These jets are important for the generation of spray above the ocean surface, which evaporates and turns into aerosols which act as cloud-formation nuclei. Kientzler *et al.* (1954) performed an early study with a 3000 fps 16-mm high-speed film camera. MacIntyre (1972), Boulton-Stone & Blake (1993) and Duchemin *et al.* (2002) performed numerical simulations of this jetting process.

Renewed interest in this phenomenon has been driven by commercial beverage applications. The crater jets are clearly visible rising from the surface of soft drinks or champagne, producing the familiar fizzy sound of freshly poured beverages. The details of this effervescence are of great importance to the sparkling wine industry (Séon & Liger-Belair 2017). However, for the popping bubbles the crater size is limited to the capillary length (Ghabache *et al.* 2014; Walls, Henaux & Bird 2015), which is significantly smaller than the impact craters studied herein. The scaling of the jetting is therefore dependent on the Bond number, as recently discussed by Krishnan, Hopfinger & Puthenveettil (2017). On the other hand Ganan-Calvo (2017) has scaled the size of the principal drop pinched from the jet tip, in a universal manner, using a capillary-inertial scaling in terms of an Ohnesorge number, without any contribution from gravity.

Deike *et al.* (2018) have performed the most detailed simulation of these bubble-bursting jets to date. They include both viscosity and gravity and present the results with the Bond and Laplace numbers. They find a narrow range of parameters where viscosity cuts off the self-similar collapse of the capillary wave (Duchemin *et al.* 2002) and the dynamics develop a finite-time singularity, where they suggest surface curvature and pressure diverge.

The phenomenon of some hand-held fireworks has been shown to be related, as jetting develops from gas bubble nucleation and bursting within the melt (Inoue *et al.* 2013). This can lead to a cascade of incandescent jets from the subsequent satellite droplets (Inoue *et al.* 2017).

1.3. *Open questions*

Despite decades of study, key open questions remain on the underlying dynamics of the fine singular crater jets. Rein (1996) as well as Michon *et al.* (2017) note that fast

https://doi.org/10.1017/jfm.2018.435 Published online by Cambridge University Press

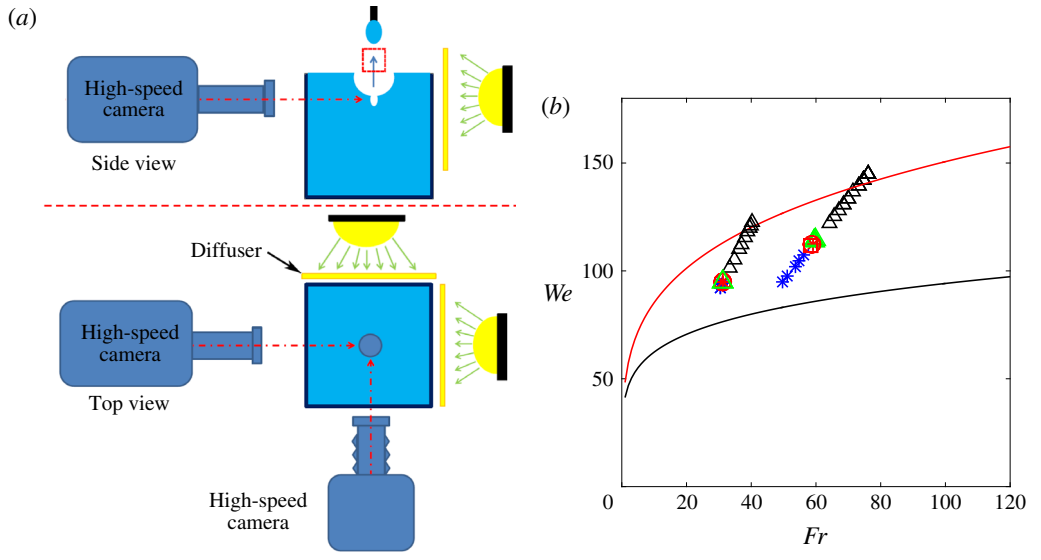


FIGURE 2. (*a*) Sketch of the experimental set-up, with two high-speed video cameras viewing the dynamics from perpendicular directions. One camera captures the dimple dynamics inside the pool, while the other views the jet droplets as they emerge out of the crater (within red square). (*b*) Our impact conditions in *Fr*–*We*-space compared to the bounds of the range of the regular bubble entrapment regime measured by Pumphrey & Elmore (1990), using the best fit curves from Oguz & Prosperetti (1990). The two linear clusters of points correspond to different drop diameters of $D = 3.3$ mm and 4.2 mm, with the larger drop at lower *Fr*. The meanings of the symbols are given graphically in figure 3.

jets can occur with or without the dimple pinching off a central bubble. Zeff *et al.* (2000) and Liow (2001) propose the fastest jets are formed by capillary retraction of the dimple without pinch-off. None of these studies had imaging with sufficient time resolution to resolve this issue. Herein we use unprecedented time and space resolution to pinpoint new aspects of these phenomena. Using 2 μs time resolution, not available to earlier studies, we show that while fast jets are generated by dimple pinch-off, the very fastest jets occur by pure inertial focusing when the dimple does not pinch-off, but its bottom rises vertically at high speed. No curvature singularity develops and the jet passes through the dimple. The dynamics thereby bypass the pinch-off singularity.

2. Experimental set-up

2.1. *Imaging set-up*

The experimental configuration is sketched in figure 2(*a*). The drop is released from a millimetric flat steel nozzle and subsequently free falls onto a pool surface, contained in a square plexiglass tank. The liquid is ∼6.5 cm deep inside of 9.4 cm × 9.4 cm inner cross-section. The drop diameters are less than 4.2 mm, so we do not expect capillary waves reflected from the walls to influence the crater collapse.

We use two synchronized ultra-high-speed video cameras (Etoh *et al.* 2003), made by Shimadzu Corp.; one was a prototype and the other a production model. One camera is used to observe the crater evolution below the free surface and the other to catch the fine jetting as it emerges from the crater and rises above the free surface.

https://doi.org/10.1017/jfm.2018.435 Published online by Cambridge University Press

The two cameras are arranged perpendicularly to each other, with each having a separate backlight diffuser. These cameras can take 102 frames at frame rates up to 1 million fps, each with 260 px × 312 px, irrespective of the frame rate. The imaging was triggered by the falling drop cutting the beam from a laser pointer, which shone on a photodiode. The two camera time delays were adjusted independently, to catch the relevant feature on the two video clips.

We use a long-distance microscope (Leica Z16 APO) for imaging the crater evolution. It has adjustable magnification and aperture. Magnifications as high as 14.6 were used herein, giving a corresponding pixel resolution of up to 2.98 μm px^{-1}. This required intense back-lighting with a Sumita metal-halide lamp, shone on a diffuser. This camera used frame rates as high as 500 kfps, which is in practice limited by the jitter in the trigger timing.

The other camera, used to observe the jetted fine droplets, had a 200 mm Nikon lens with bellows to provide added magnification, for a resolution of 20.3 μm px^{-1}. To capture the fastest jetting we use frame rates as high as 200 kfps.

2.2. *Liquids and drop shapes*

We use the same 50 % by-volume water/glycerin mixture for the drop and pool liquids. The pool and air temperatures were measured continuously with embedded thermometers and were in the range 22 °C–26 °C, which was taken into account when calculating liquid properties. For typical temperatures $T \simeq 24$ °C, this gives liquid density $\rho = 1140$ kg m^{-3}, dynamic viscosity $\mu = 7.13 \times 10^{-3}$ Pa s and the corresponding kinematic viscosity $\nu = 6.25 \times 10^{-6}$ m^2 s^{-1}. The surface tension is $\sigma = 0.065$ N m^{-1}. The illumination is blocked between impacts, but a minor temperature difference can arise from the intense lighting and cause a slight difference in the index of refraction between drop and pool, when viewing tangentially along their interface. This becomes visible as a faint line separating the two liquids in the video images.

Some initial experiments were performed with deionized water, but the craters were too variable to allow for repeatable trigger timing, which is needed for the short-duration video clips of our cameras.

The drop is pinched off from one of two tapered stainless steel nozzles with a sharp inner edge of ∼1.2 or 1.8 mm in diameter, producing droplets with diameters of 3.33 mm and 4.20 mm, respectively. The impact velocities and droplet shapes were measured from the top camera. The elevated viscosity, from that of water, quickly reduces oscillations from the pinch-off during the free-fall, with the drop being axisymmetric. However, some shape-oscillations remain, which we characterize by giving the aspect ratio $\alpha = D_V/D_H$, where D_H and D_V are the horizontal and vertical diameters, respectively, at impact. The equivalent spherical drop diameter is estimated as $D = (D_V D_H^2)^{1/3}$. The aspect ratio varies between 0.95 and 1.05. The release height H, measured from the nozzle to the pool surface, was varied in the range $H \simeq 6$–12 cm, giving impact velocities in the range $U \simeq 1.1$–1.6 m s^{-1}.

2.3. *Parameter space*

We characterize the impact conditions by the Reynolds, Weber and Froude numbers,

$$Re = \frac{\rho D U}{\mu}, \quad We = \frac{\rho D U^2}{\sigma}, \quad Fr = \frac{U^2}{gD}, \tag{2.1a–c}$$

https://doi.org/10.1017/jfm.2018.435 Published online by Cambridge University Press

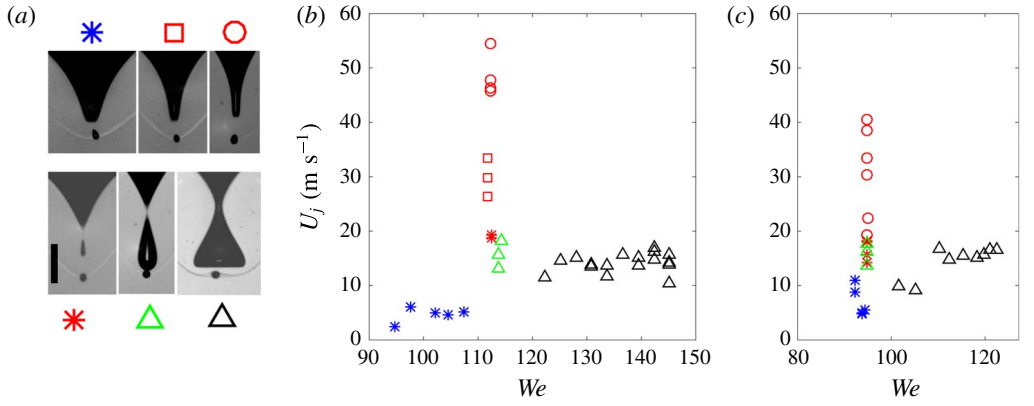


FIGURE 3. Jetting velocity U_j versus impact *We* spanning the range of dimple collapse. (*a*) The symbols corresponding to different dimple shapes. Scale bar is 500 μm. No pinch-off shallow angled dimple (∗, blue). Weakly singular jet (□, red). Singular jet (○, red). Small bubble pinched off (∗, red). Teardrop pinch-off (△, green). Conical dimple pinch-off (△). (*b*,*c*) Jet velocities versus impact *We*, for two different drop sizes of $D = 3.33$ mm in (*b*) and for $D = 4.20$ mm in (*c*).

where g is the acceleration of gravity. Note that this definition of *Fr*, without the square root, is used in the relevant earlier studies on this topic. Figure 2(*b*) shows where our impact conditions fall in the classical regime constructed by Pumphrey & Elmore (1990) and fitted by Oguz & Prosperetti (1990), which shows where the regular entrapment of a bubble at the crater centre occurs. Our data overlap, on the upper *We* range, but no bubble entrapment occurs for our blue stars. This discrepancy is not surprising, as our liquid is more viscous than in those studies. This is consistent with the trends observed by Deng *et al.* (2007). Our *Re* are always in the range from 700 to 900.

3. Results

3.1. *Dimple shapes and jetting speeds*

We focus on the crater collapse when a dimple forms at its bottom and fine jets are produced. Figure 3(*a*) shows how we categorize the dimple shapes which appear. During the crater collapse, capillary waves travel from the rim down towards the bottom centre. They can form conical shapes without pinching off a bubble (∗, blue). As we increase the impact velocity these cones become sharper and eventually form a narrow vertical cylinder, which produces what we term singular jetting (○, red). This occurs in a narrow range of U or *We*, shown in figure 3. Past this regime we observe regular pinch-off of large bubbles with $D_b \sim 300$–500 μm. We split this into teardrop (△, green) and triangular pinch-off (△). While the singular jets occur at almost the same *We* as the small-bubble pinch-off (∗, red) there is no ambiguity regarding the jetting speed for each case, as we have simultaneous viewing of the jet and the dimple.

Note that the small bubble of ∼80 μm in diameter, sitting under the dimple in figures 3 and 4, is due to the air-disc entrapped under the centre of the drop, when it first contacts the pool, as was studied by Thoroddsen *et al.* (2003). This bubble sits along the faint line separating the drop and pool liquids (see § 2.2). It is telling about

https://doi.org/10.1017/jfm.2018.435 Published online by Cambridge University Press

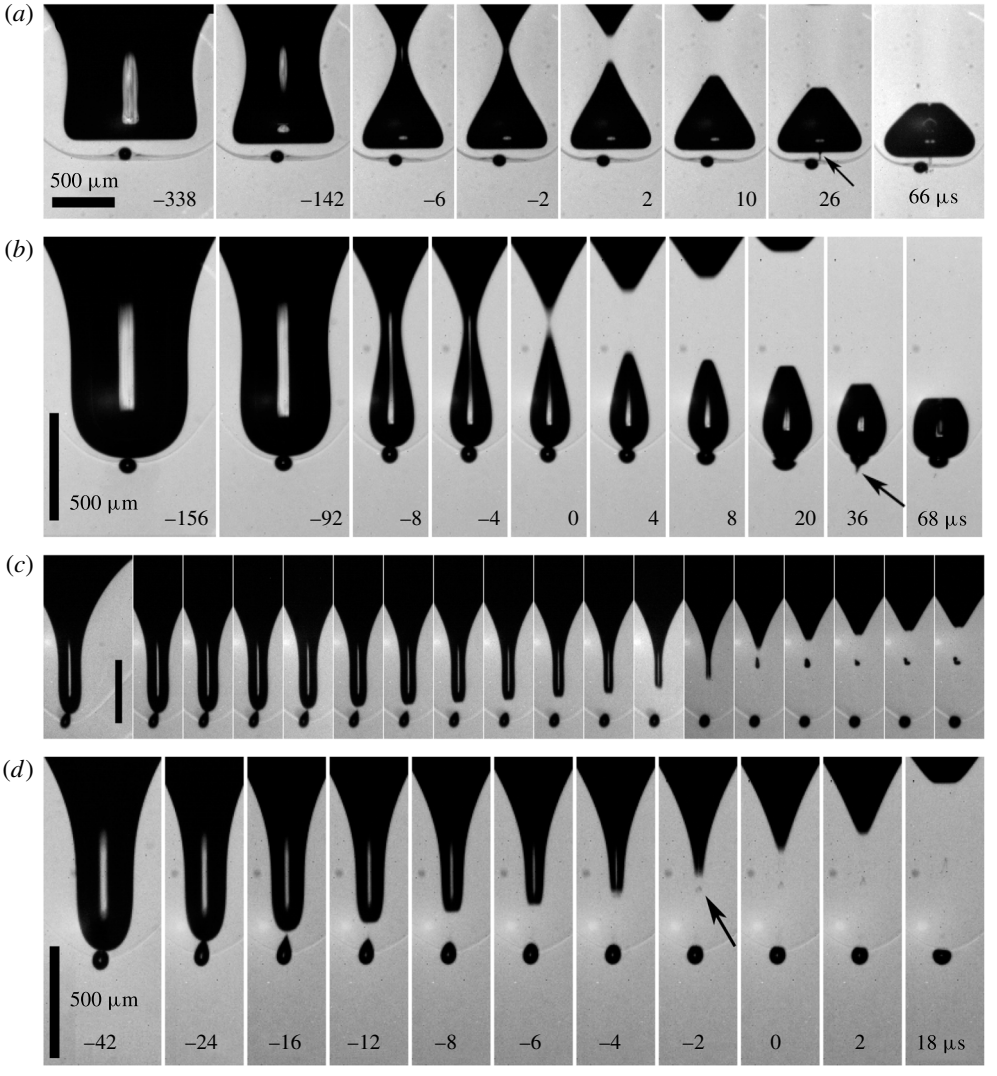


FIGURE 4. Typical dimple collapse for different impact conditions. The small bubble, sitting below the dimple at the start of each sequence, is the central bubble entrapped under the drop as it first impacts the pool (Thoroddsen, Takehara & Etoh 2003). (*a*) Triangular necking. The arrow indicates a fine jet, produced by the pinch-off, which penetrates through the bottom of the bubble. $U = 1.27$ m s^{-1}, $D = 4.20$ mm, $We = 118$, $Fr = 39$ and $Re = 895$. (*b*) Teardrop necking. The arrow indicates the penetrating downwards jet. $U = 1.40$ m s^{-1}, $D = 3.33$ mm, $We = 114$, $Fr = 60$ and $Re = 783$. (*c*) Cylindrical dimple collapse, with a small bubble pinched off. The pinched-off bubble splits into two small bubbles. The time between frames is 2 μs and scale bar is 500 μm. $U = 1.13$ m s^{-1}, $D = 4.20$ mm, $We = 95$, $Fr = 31$ and $Re = 801$. (*d*) Cylindrical dimple singular collapse. The arrow indicates micro-bubbles formed at the end of the rapidly moving bottom. $U = 1.39$ m s^{-1}, $D = 3.33$ mm, $We = 112$, $Fr = 59$ and $Re = 776$. See also supplementary movies 1–4, which are available at https://doi.org/10.1017/jfm.2018.435.

https://doi.org/10.1017/jfm.2018.435 Published online by Cambridge University Press

the image resolution of earlier studies that this unavoidable central entrapped bubble is not visible in most of them.

Figure 3(*b*,*c*) show how the jetting velocity U_j changes for the different dimple pinch-off shapes, as we increase U and thereby We. Both drop diameters show the same trend. These velocities are measured from the first droplets which emerge out of the crater, which we presume originate from the tip of the narrow jet, as it breaks up by Rayleigh instability. For the fast jets we typically see 20 micro-droplets. U_j spikes at a narrow range of We, where it reaches a fourfold velocity compared to the surrounding conditions. This higher velocity coincides with the singular cylinder, where no bubble is pinched off. This occurs at $We = 112$ for the smaller drop and at $We = 95$ for the larger drop. The corresponding values of $Fr \simeq 60$ and 30 are much smaller than in other studies (Michon *et al.* 2017).

Figure 4 shows the details of the dimple collapse and pinch-off. The sequences of frames have a time resolution of 2 or 4 μs. The necking collapse in figure 4(*a*) produces two fine Worthington jets, which travel up and down from the neck. The downwards travelling jet penetrates the bottom of the bubble, in the seventh image, as is marked by the arrow. We can estimate the speed of this downwards jet by measuring the distance from the neck to the bottom of the bubble and dividing by the 25 μs duration of this travel. This gives a repeatable velocity over a few realizations of $u_j = 36.2 \pm 4.2$ m s^{-1}. We estimate the width of this jet to be ∼15 μm. Keep in mind that the flat bottom of the bubble shadow does not mean the bubble is flat, and indeed the bottom appears to be bent upwards at the centreline. Similar jet speeds are seen for the teardrop pinch-off in panel (*b*). Panel (*c*) shows a near-singular pinch-off where only a small bubble is pinched off. Figure 3 showed that any pinch-off greatly reduces the jetting velocity – even the tiny bubble in figure 4(*c*). Finally, panel (*d*) shows singular retraction of the tip, which corresponds to the largest jetting velocities.

The faint line visible in the images separates the drop and pool liquids and arises most likely from slight differences in temperature between the two, as explained in § 2.2. This shows that the fast jets contain only drop liquid (Gekle & Gordillo 2010).

3.2. *Power laws for collapse of dimple radius*

The final pinch-off of the dimple was recorded at up to 500 kfps, which allows us to track the dimple radii versus time to reveal the power-law behaviour near the final pinch-off,

$$R(t) = C(t_o - t)^{\beta}, \tag{3.1}$$

where t_o is our estimate of the pinch-off time. C is a fitting parameter, which becomes independent of σ and gravity at the smallest scales. For the conical dimple we follow the minimum radius, whereas for the teardrop pinch-off we follow the radius at the depth of the final pinch-off. Figure 5 shows that for both cases the exponents are closer to 1/2 for inertial collapse, than to the capillary-inertial dynamics, which should follow a slope of 2/3. The values of the exponents are close to those observed for bubble pinch-off from rest in Thoroddsen, Etoh & Takehara (2007*a*).

Figure 6(*a*) traces the radial collapse and vertical retraction of the singular cylindrical dimple, like the one shown in figure 4(*d*). Here the dimple has an almost vertical wall, so its radius is well defined. In other cases the wall is more cone-shaped and we measure the radius at a fixed z-location, where the maximum vertical retraction speed $\mathrm{d}z/\mathrm{d}t$ occurs, which we also select as time t_o. When the cylinder becomes narrowest its bottom moves up most rapidly, but its width does

https://doi.org/10.1017/jfm.2018.435 Published online by Cambridge University Press

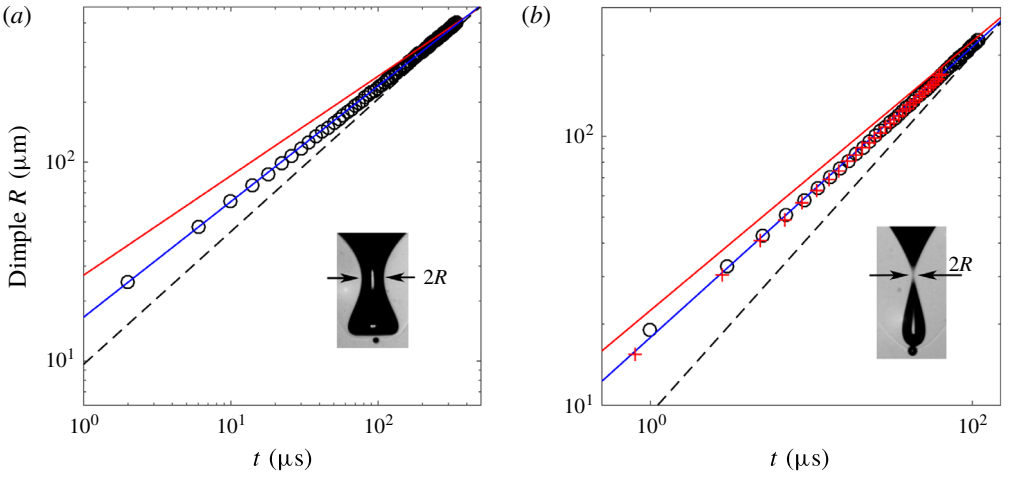


FIGURE 5. Radial collapse of the dimple pinch-off. The dashed lines correspond to capillary-inertial dynamics with a slope of 2/3, while the solid red lines correspond to inertial focusing at slope of 1/2. (*a*) The pinch-off of a conical dimple, with an exponent of $\beta = 0.58 \pm 0.02$ (blue line). (*b*) Two realizations for the radius of teardrop pinch-off from 500 kfps, giving power-law exponent near pinch-off of $\beta = 0.54 \pm 0.02$ (blue line).

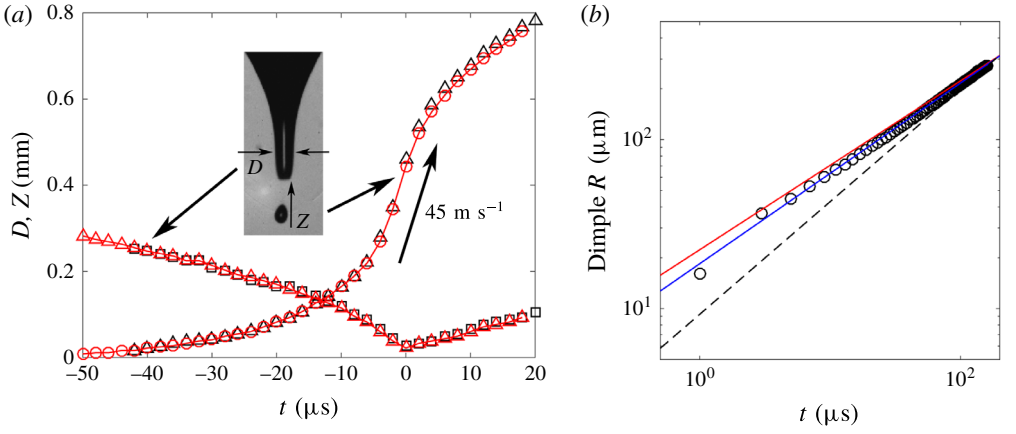


FIGURE 6. Radial collapse of the singular dimple cylinder. (*a*) The diameter of the tip and the vertical motion of the bottom Z of the air cylinder. (*b*) The radius of bottom cylinder taken from 500 kfps video. The best fit line gives a power-law exponent near pinch-off of $\beta = 0.535 \pm 0.02$ (blue line). The dashed line corresponds to capillary-inertial dynamics with a slope of 2/3, while the solid red line corresponds to inertial focusing of slope 1/2.

not go through a singularity, rather reaching here a minimum radius of $R \simeq 11$ μm, which we propose coincides with the formation of the vertical fine jet. Following this the edge of the cylinder widens again at a slow rate. Figure 6(*b*) shows that the radius again follows an inertial power law with exponent $\beta = 0.53 \pm 0.02$, with the caveat that selecting t_o is somewhat arbitrary in this case.

https://doi.org/10.1017/jfm.2018.435 Published online by Cambridge University Press

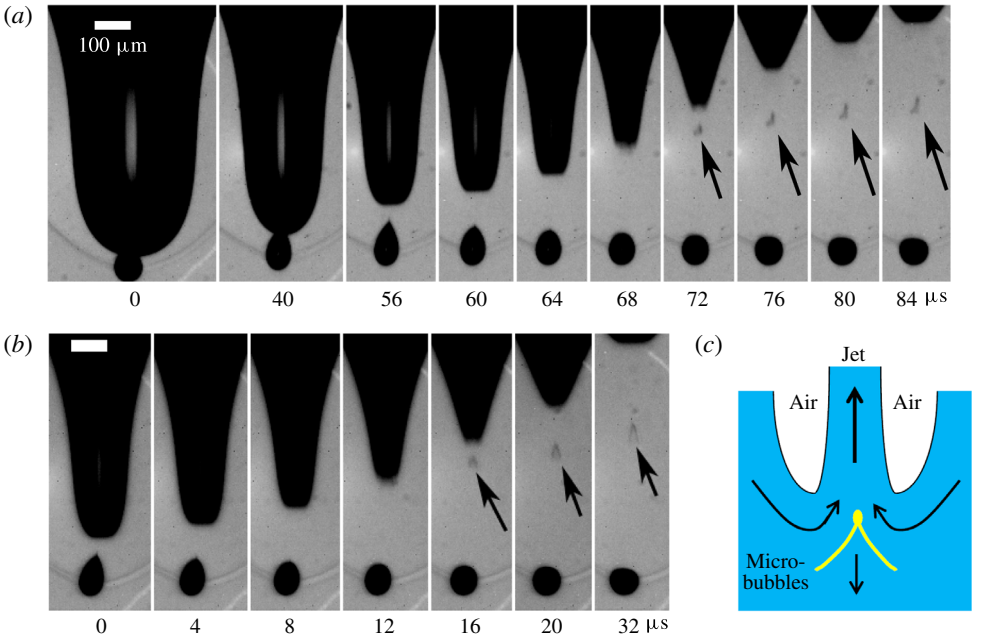


FIGURE 7. Two realizations showing rapidly retracting cylindrical bottom dimples, shedding micro-bubbles, as indicated by the arrows. The scale bars are both 100 μm. See also supplementary movies 5 and 6.

The arrow in figure 4(*d*) identifies a faint group of micro-bubbles separating from the tip of the air cylinder. Figure 7 shows close-up images of this phenomenon, where the rapidly pulled up air cylinder leaves behind a small conical region of micro-bubbles, indicated by the arrows. This dark feature has a characteristic conical shape with its apex reaching into the jet base, indicating its direction. We suggest this structure forms slightly behind the jet, which itself is driven by the high pressure from the inertial focusing. Immediately following this ejection the flow which turns sharply around the jet base, as is sketched in (*c*), could separate, generating low pressure, and cavitate the liquid. This micro-bubble signature is faint, but it occurs in a repeatable fashion.

3.3. *Bubble compression and sound generation*

Note the sudden apparent volume expansion of the bubble, in figure 4(*b*), between times 4 and 20 μs after the pinch-off. The supplementary movies 2 and 7 show clearly the subsequent cycles of compression and expansion of the bubble. If we assume axisymmetry of the bubble and ignore the volume of the fine jet we can obtain a rough estimate of the volume compression. This ratio varies widely, but in some cases it exceeds a factor of 2.5, as in the case shown in figure 8 when comparing frames 5 and 7. The amplitude in subsequent oscillations will rapidly reduce by viscous dissipation. This suggests excess pressure above atmospheric. The oscillation of this bubble has indeed been shown to be the source of the underwater sound of rain on the ocean (Oguz & Prosperetti 1990; Pumphrey & Elmore 1990; Oguz & Prosperetti 1991; Prosperetti & Oguz 1993), using hydrophones. Here we can measure the oscillation frequency directly from the video. From numerous such

https://doi.org/10.1017/jfm.2018.435 Published online by Cambridge University Press

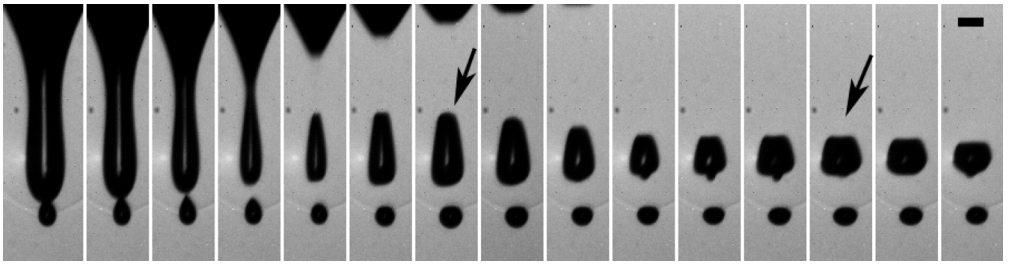


FIGURE 8. Compression of the pinched-off bubble. Time between frames is 4 μs and the scale bar is 100 μm long. The arrows indicate the maximum bubble volume during the expansion phase. See also supplementary movie 7.

identical measurements we obtain 23 ± 2 kHz, which is slightly above the audible range, which reaches 20 kHz. The rain-produced sound energy in the ocean has a peak at 14 kHz (Prosperetti & Oguz 1993). Keep in mind that the bubble diameter in figure 8 is only approximately 170 μm and the frequency will be inversely proportional to size. However, this demonstrates the potential power of this direct imaging, which could be acquired along-side hydrophone records.

4. Discussion and conclusions

We conclude that the most singular jets arise from inertia focusing, without bubble pinch-off. This is consistent with the seminal results of Zeff *et al.* (2000), who observed their fastest jets without pinch-off. However, the free-surface dynamics are not self-similar and divergent surface tension is not the driving mechanism, as they suggested and was explained by Brenner (2000). See also the follow-up study by Das & Hopfinger (2008), who suggest inertial focusing, but did not have time-resolved imaging to capture the fastest jets. We further verify this by tracking the collapse of the final dimple radius, in figure 6, which reveals power law $\beta \simeq 0.55$ with close to the pure inertial exponent of $1/2$ as is observed for bubble pinch-offs (Burton, Waldrep & Taborek 2005; Keim *et al.* 2006; Thoroddsen *et al.* 2007*a*). Indeed measuring values slightly larger than 0.5 is expected, as the transition in the value of the exponent from capillary-driven to inertial-driven dynamics, in bubble pinch-off, is known to be logarithmically slow (Gordillo *et al.* 2005; Bergmann *et al.* 2006; Eggers *et al.* 2007).

The finest jets are much thinner and faster than would have been possible to observe in most of the previous studies. Here we observe the fastest droplets jetting at velocities $\sim$50 m s^{-1} when they emerge out of the crater, while Deng *et al.* (2007) saw a maximum of 15 m s^{-1}, Ghabache *et al.* (2014) saw 14 m s^{-1} and Liow (2001) measured 10.5 m s^{-1}. These are certainly all underestimates, as the very small tip droplets are greatly decelerated by air drag before they emerge out of the crater and the initial speed of the jets will therefore be even larger. Typical deceleration is shown for a representative droplet in the supplementary materials. This explains why the early downwards jets for the teardrop pinch-off, in figure 4(*b*), are much faster (35 m s^{-1}) than those emerging out of the crater at 19 m s^{-1}. Extrapolating this, the singular jets may be generated at closer to 100 m s^{-1}. Observations by X-rays, of the jet inside the dimple, would be very useful but are currently not available at such high frame rates (Zhang *et al.* 2012). Pinning down the diameter and speed of the very finest droplets will require even finer time and space resolution.

https://doi.org/10.1017/jfm.2018.435 Published online by Cambridge University Press

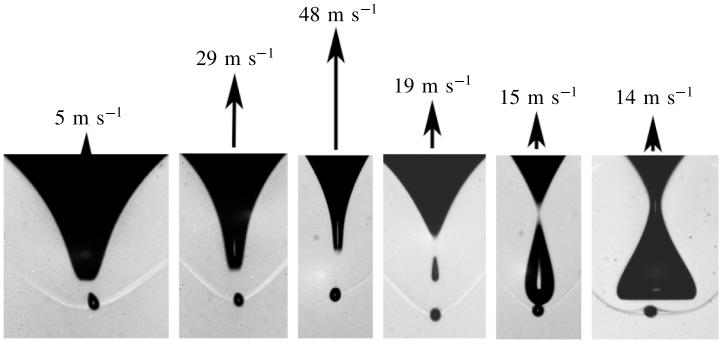


FIGURE 9. Schematic of jetting speeds versus dimple shapes, corresponding to figure 3. The arrow lengths indicate the jet velocities. The Weber number grows from left to right.

Intuitively, one might expect the radial collision of the dimple walls to produce the fastest jets, in a similar way as for the fine Worthington jets produced by the collapse of sphere-impact cavities (Worthington & Cole 1897; Gekle *et al.* 2009; Gekle & Gordillo 2010). But this is not the case in our configuration. Figure 9 graphically summarizes the jetting speed results. The fastest jets occur at the lower bound of the bubble pinch-off regime. At *We* below this boundary we find broader conical dimples with much slower jetting. Closer to the first pinch-off the dimple cylinder becomes steeper, forming faster and faster jets. Once pinch-off occurs the jetting speed drops greatly. In essence the flow bypasses a singularity, but tries to get as close as possible. This leaves open the question, whether there exists an even finer tuning which will produce still faster jets, or will this be mitigated by cavitation? The sketch in figure 7 indicates the overall flow field at the base of the jet, which contains a stagnation point with high pressure required to drive the jet through the bottom of the dimple; see also the sketch in Ganan-Calvo (2017). Figure 8 also underscores the large induced pressure by the very strong compression of the gas, observed when the bottom dimple is pinched off. While the inertial focusing will produce high pressure at the base of the dimple to drive the fine jet, figure 7 shows intriguing clues for extreme suction pressure in the region near the base of the jet, by the formation of micro-bubbles. These bubbles could be pulled from the free surface, but we speculate cavitation could be at play. The flow is extremely transient and the rapid motions of a curved free surface are known to generate vorticity which can play a role here, as shown by Thoraval *et al.* (2012). Indeed, the very strong extensional forces, suggested by the formation of these micro-bubbles in figure 7, may be important for damaging cells in bioreactors when bubbles pop at free surfaces, as has been suggested by Tran *et al.* (2016) and Walls *et al.* (2017).

There is clearly need for further study of the details of the flow fields during the dimple collapse with fully resolved simulations and theory, in the vein of Morton *et al.* (2000), Gekle & Gordillo (2010), Ray *et al.* (2015), Walls *et al.* (2015) and Deike *et al.* (2018).

In summary, herein we have shown that the fastest thin jets bypass the dimple pinch-off singularity and are driven purely by inertial focusing.

Acknowledgement

The work reported herein was partly funded by King Abdullah University of Science and Technology (KAUST) under grant URF/1/2621-01-01.

https://doi.org/10.1017/jfm.2018.435 Published online by Cambridge University Press

Supplementary movies

Supplementary movies are available at https://doi.org/10.1017/jfm.2018.435.

References

BERGMANN, R., VAN DER MEER, D., STIJNMAN, M., SANDTKE, M., PROSPERETTI, A. & LOHSE, D. 2006 Giant bubble pinch-off. *Phys. Rev. Lett.* **96**, 154505.

BOULTON-STONE, J. M. & BLAKE, J. R. 1993 Gas bubbles bursting at a free surface. *J. Fluid Mech.* **254**, 437–466.

BRENNER, M. P. 2000 Jets from a singular surface. *Nature* **403**, 377–378.

BURTON, J. C., WALDREP, R. & TABOREK, P. 2005 Scaling and instabilities in bubble pinch-off. *Phys. Rev. Lett.* **94**, 184502.

DAS, S. P. & HOPFINGER, E. J. 2008 Parametrically forced gravity waves in a circular cylinder and finite-time singularity. *J. Fluid Mech.* **599**, 205–228.

DEIKE, L., GHABACHE, E., LIGER-BELAIR, G., DAS, A. K., ZALESKI, S., POPINET, S. & SÉON, T. 2018 Dynamics of jets produced by bursting bubbles. *Phys. Rev. Fluids* **3**, 013603.

DENG, Q., ANILKUMAR, V. & WANG, T. G. 2007 The role of viscosity and surface tension in bubble entrapment during drop impact onto a deep liquid pool. *J. Fluid Mech.* **578**, 119–138.

DUCHEMIN, L., POPINET, S., JOSSERAND, C. & ZALESKI, S. 2002 Jet formation in bubbles bursting at a free surface. *Phys. Fluids* **14**, 3000–3008.

EGGERS, J., FONTELOS, M. A., LEPPINEN, D. & SNOEIJER, J. 2007 Theory of the collapsing axisymmetric cavity. *Phys. Rev. Lett.* **98**, 094502.

ETOH, T. G. *et al.* 2003 An image sensor which captures 100 consecutive frames at 1000 000 frames s^{-1}. *IEEE Trans. Electron Devices* **50**, 144–151.

GANAN-CALVO, A. M. 2017 Revision of bubble bursting: universal scaling laws of top jet drop size and speed. *Phys. Rev. Lett.* **119**, 204502.

GEKLE, S. & GORDILLO, J. M. 2010 Generation and breakup of Worthington jets after cavity collapse. Part 1. Jet formation. *J. Fluid Mech.* **663**, 293–330.

GEKLE, S., GORDILLO, J. M., VAN DER MEER, D. & LOHSE, D. 2009 High-speed jet formation after solid object impact. *Phys. Rev. Lett.* **102**, 034502.

GHABACHE, E., ANTKOWIAK, A., JOSSERAND, C. & SÉON, T. 2014 On the physics of fizziness: how bubbles bursting controls droplets ejection. *Phys. Fluids* **26**, 121701.

GORDILLO, J. M., SEVILLA, A., RODRÍGUEZ-RODRÍGUEZ, J. & MARTÍNEZ-BAZÁN, C. 2005 Axisymmetric bubble pinch-off at high Reynolds numbers. *Phys. Rev. Lett.* **95**, 194501.

INOUE, C., IZATO, Y., MIYAKE, A. & VILLERMAUX, E. 2017 Direct self-sustained fragmentation cascade of reactive droplets. *Phys. Rev. Lett.* **118**, 074502.

INOUE, C., KOSHI, M., TERASHIMA, H., HIMENO, T. & WATANABE, T. 2013 Origin of droplets in sparkling fireworks. *Sci. Technol. Energetic Mater.* **74**, 106–111.

KEIM, N. C., MOLLER, P., ZHANG, W. W. & NAGEL, S. N. 2006 Breakup of air bubbles inwater: memory and breakdown of cylindrical symmetry. *Phys. Rev. Lett.* **97**, 144503.

KIENTZLER, C. F., ARONS, A. B., BLANCHARD, D. C. & WOODCOCK, A. H. 1954 Photographic investigation of the projection of droplets by bubbles bursting at a water surface. *Tellus* **6**, 1–7.

KRISHNAN, S., HOPFINGER, E. J. & PUTHENVEETTIL, B. A. 2017 On the scaling of jetting from bubble collapse at a liquid surface. *J. Fluid Mech.* **822**, 791–812.

LIOW, L. J. 2001 Splash formation by spherical drops. *J. Fluid Mech.* **427**, 73–105.

MACINTYRE, F. 1972 Flow patterns in breaking bubbles. *J. Geophys. Res.* **77**, 5211–5228.

MICHON, G.-J., JOSSERAND, C. & SÉON, T. 2017 Jet dynamics post drop impact on a deep pool. *Phys. Rev. Fluids* **2**, 023601.

MORTON, D., RUDMAN, M. & LIOW, J.-L. 2000 An investigation of the flow regimes resulting from splashing drops. *Phys. Fluids* **12**, 747–763.

OGUZ, H. N. & PROSPERETTI, A. 1990 Bubble entrainment by the impact of drops on liquid surfaces. *J. Fluid Mech.* **219**, 143–179.

https://doi.org/10.1017/jfm.2018.435 Published online by Cambridge University Press

OGUZ, H. N. & PROSPERETTI, A. 1991 Numerical calculation of the underwater noise of rain. *J. Fluid Mech.* **228**, 417–442.

PROSPERETTI, A. & OGUZ, H. N. 1993 The impact of drops on liquid surfaces and the underwater noise of rain. *Annu. Rev. Fluid Mech.* **25**, 577–602.

PUMPHREY, H. C. & ELMORE, P. A. 1990 The entrainment of bubbles by drop impacts. *J. Fluid Mech.* **220**, 539–567.

RAY, B., BISWAS, G. & SHARMA, A. 2015 Regimes during drop impact on a liquid pool. *J. Fluid Mech.* **768**, 492–523.

REIN, M. 1996 The transition regime between coalescing and splashing drops. *J. Fluid Mech.* **306**, 145–165.

SÉON, T. & LIGER-BELAIR, G. 2017 Effervescence in champagne and sparkling wines: from bubble bursting to droplet evaporation. *Eur. Phys. J. Special Top.* **226**, 117–156.

THORAVAL, M.-J., TAKEHARA, K., ETOH, T. G., POPINET, S., RAY, P., JOSSERAND, C., ZALESKI, S. & THORODDSEN, S. T. 2012 Von Kármán vortex street within an impacting drop. *Phys. Rev. Lett.* **108**, 264506.

THORODDSEN, S. T., ETOH, T. G. & TAKEHARA, K. 2007*a* Experiments on bubble pinch-off. *Phys. Fluids* **19**, 042101.

THORODDSEN, S. T., ETOH, T. G. & TAKEHARA, K. 2007*b* Micro-jetting from wave-focusing on oscillating drops. *Phys. Fluids* **19**, 052101.

THORODDSEN, S. T., TAKEHARA, K. & ETOH, T. G. 2003 Air entrapment under an impacting drop. *J. Fluid Mech.* **478**, 125–134.

TRAN, T. T., LEE, E. G., LEE, I. S., WOO, N. S., HAN, S. M., KIM, Y. J. & HWANG, W. R. 2016 Hydrodynamic extensional stress during the bubble bursting process for bioreactor system design. *Korea-Aust. Rheol. J.* **28**, 315–326.

WALLS, P. L. L., HENAUX, L. & BIRD, J. C. 2015 Jet drops from bursting bubbles: how gravity and viscosity couple to inhibit droplet production. *Phys. Rev.* E **92**, 021002(R).

WALLS, P. L. L., MCRAE, O., NATARAJAN, V., JOHNSON, C., ANTONIOU, C. & BIRD, J. C. 2017 Quantifying the potential for bursting bubbles to damage suspended cells. *Sci. Rep.* **7**, 15102.

WORTHINGTON, A. M. & COLE, R. S. 1897 Impact with a liquid surface, studied by the aid of instantaneous photography. *Phil. Trans. R. Soc. Lond.* A **189**, 137–148.

ZEFF, B. W., KLEBER, B., FINEBERG, J. & LATHROP, D. P. 2000 Singularity dynamics in curvature collapse and jet eruption on a fluid surface. *Nature* **403**, 401–404.

ZHANG, F., THORAVAL, M.-J., THORODDSEN, S. T. & TABOREK, P. 2015 Partial coalescence from bubbles to drops. *J. Fluid Mech.* **782**, 209–239.

ZHANG, L. V., TOOLE, J., FEZZAA, K. & DEEGAN, R. D. 2012 Evolution of the ejecta sheet from the impact of a drop with a deep pool. *J. Fluid Mech.* **690**, 5–15.

https://doi.org/10.1017/jfm.2018.435 Published online by Cambridge University Press